

# POLITECNICO DI TORINO

Corso di Laurea Magistrale in Automotive Engineering

Tesi di Laurea Magistrale

Investigating pressure drops and flow uniformity in fuel cell flow channels.



**Politecnico  
di Torino**



**Relatore:**

Assoc. Prof. Özgür Ekici (Hacettepe University)

**Candidato:**

Musa Abbasov

**Correlatore:**

Prof. Misul Daniela Anna

A.A. 2021/2022

## ABSTRACT

High energy efficiency, being lightweight, quick start-up, and lower operating temperature make polymer electrolyte membrane fuel cells an excellent choice for automobiles. These devices can be more dependable and efficient in the long run if flow field plates continue to improve in the areas of reactant distribution, lower pressure drops, accurately optimized water content, and better heat management. The influence of a single serpentine flow field configuration with two different active areas on pressure drop and flow uniformity was studied numerically and analytically in this study. This was done first by developing the flow field pattern in "SolidWorks", and then by running simulations to see how the flow channel performed using commercial CFD software, "ANSYS FLUENT". Before running the simulations, a preliminary set-up is completed, which involves verifying the SolidWorks structures with "DesignModeler" and creating the mesh. An improved method of mesh selection is employed in order to identify the most effective mesh among those considered. In order to verify the numerical predictions, an analytical analysis is carried out on flow field configurations. The comparison of numerical and analytically generated pressure drop data showed that they agreed well with the existing literature. Finally, a number of modifications have been put to the test to see whether they can reduce pressure drop. Consequently, the pressure drops were less than the single serpentine flow field design we started with.

**Keywords:** PEM fuel cell, Flow channel design, Serpentine flow field, CFD modelling, Pressure drop.

# TABLE OF CONTENTS

<b>ABSTRACT .....</b>	<b>II</b>
<b>LIST OF FIGURES .....</b>	<b>V</b>
<b>LIST OF TABLES .....</b>	<b>VI</b>
<b>NOMENCLATURE .....</b>	<b>VII</b>
<b>INTRODUCTION .....</b>	<b>1</b>
<b>1. The Polymer Electrolyte Membrane Fuel Cell's Primary Components .....</b>	<b>2</b>
1.1. Membrane Electrode Assembly (MEA) .....	3
1.2. Bipolar Plates .....	5
1.2.1. Fundamental Flow Field Designs .....	6
1.2.2. Nature-inspired Flow Field Designs .....	8
1.2.3. Hybrid Flow Field Designs .....	8
<b>2. The PEM Fuel Cell's Fundamental Operation .....</b>	<b>9</b>
<b>LITERATURE REVIEW .....</b>	<b>11</b>
<b>1. Fundamental designs.....</b>	<b>11</b>
<b>2. Nature-inspired designs.....</b>	<b>13</b>
<b>3. Thesis Objective .....</b>	<b>14</b>
<b>THEORY AND MODELLING.....</b>	<b>15</b>
<b>1. Analytical Analysis.....</b>	<b>15</b>
<b>2. Governing Equations .....</b>	<b>17</b>
2.1. Continuity Equation .....	18
2.2. Momentum Equation .....	18
2.3. Energy Equation.....	19
<b>3. Model Development.....</b>	<b>19</b>
3.1. Simulation Technique .....	20
3.2. Mesh .....	21
3.2.1. Mesh Independence Study .....	21
3.3. Serpentine Channel with Active Area of 4x4 cm <sup>2</sup> .....	28
3.3.1. Problem Domain .....	29
3.3.2. Model Assumptions .....	30

3.3.3. Boundary Conditions .....	31
3.4. Serpentine Channel with Active Area of 10x10 cm <sup>2</sup> .....	31
3.4.1. Problem Domain .....	33
3.4.2. Model Assumptions .....	33
3.4.3. Boundary Conditions .....	33
<b>RESULTS AND DISCUSSION .....</b>	<b>35</b>
<b>1. Analytical Validation .....</b>	<b>35</b>
1.1. Serpentine Channel with Active Area of 4x4 cm <sup>2</sup> .....	35
1.2. Serpentine Channel with Active Area of 10x10 cm <sup>2</sup> .....	36
<b>2. Numerical Validation.....</b>	<b>37</b>
2.1. Serpentine Channel with Active Area of 4x4 cm <sup>2</sup> .....	37
2.1.1. Single Serpentine Channel.....	37
2.1.2. Single Serpentine Channel Modifications.....	39
2.2. Serpentine Channel with Active Area of 10x10 cm <sup>2</sup> .....	41
<b>CONCLUSION .....</b>	<b>45</b>
<b>REFERENCES .....</b>	<b>47</b>

## LIST OF FIGURES

Figure 1. Design and fabrication of a PEM fuel cell stack [3].	3
Figure 2. Structure of a membrane electrode assembly [5].	4
Figure 3. The most common flow field designs used in PEMFCs.	6
Figure 4. A representation of fractal and biological structures in schematic form [8].	8
Figure 5. Hybrid flow field designs: (a) nature-inspired and interdigitated, (b) nature-inspired and parallel [13].	9
Figure 6. A PEM fuel cell's transportation procedure [14].	10
Figure 7. Graphical representation of mesh independence study.	24
Figure 8. A portion of meshed geometry: (a) mesh size: 0.55, (b) mesh size: 0.35, (c) mesh size: 0.15	25
Figure 9. Entrance region and fully developed flow. [16]	27
Figure 10. "4x4" Serpentine flow-field design in a bipolar plate. [10]	29
Figure 11. "4x4" model: Curvature (left) and Double inlet (right)	30
Figure 12. "10x10" Serpentine flow-field design in a bipolar plate. [14]	32
Figure 13. Numerical validation of a single serpentine channel of the "4x4" model with sharp corners.	39
Figure 14. Numerical (CFD) analysis results of pressure drop in different configurations of the "4x4" model.	40
Figure 15. Numerical (CFD) analysis of "10x10" model pressure drop results for different working fluid.	42
Figure 16. Numerical (CFD) analysis of pressure drop results in different curves [14].	43
Figure 17. Numerical validation of a single serpentine channel of the "10x10" model with sharp corners and working fluid being oxygen.	44

## LIST OF TABLES

<i>Table 1. Results of the mesh independence study. ....</i>	<i>22</i>
<i>Table 2. Primary dimensions for the “4x4” model. ....</i>	<i>30</i>
<i>Table 3. Boundary conditions for the “4x4” model and for its modifications. ....</i>	<i>31</i>
<i>Table 4. Primary dimensions for the “10x10” model. ....</i>	<i>33</i>
<i>Table 5. Boundary conditions for “10x10” model. ....</i>	<i>34</i>
<i>Table 6. Reynolds Number for “4x4” model. ....</i>	<i>35</i>
<i>Table 7. Necessary Analysis Parameters for “4x4” model. ....</i>	<i>36</i>
<i>Table 8. Reynolds Number for “10x10” model. ....</i>	<i>36</i>
<i>Table 9. Necessary Analysis Parameters for “10x10” model. ....</i>	<i>36</i>

## NOMENCLATURE

---

Abbreviation	Definition
AFC	Alkaline fuel cell
BP	Bipolar plate
CAD	Computer-aided design
CFD	Computational fluid dynamics
CL	Catalyst layer
FC	Fuel cell
GDL	Gas diffusion layer
MCFC	Molten carbonate fuel cell
MEA	Membrane electrode assembly
PAFC	Phosphoric acid fuel cell
PEM	Polymer electrolyte membrane
PEMFC	Polymer electrolyte membrane fuel cell
PFSA	Perfluorosulfonic acid
V	Control volume
S	Control surface
SOFC	Solid oxide fuel cell

---

Symbol	Definition	Unit
$A$	Channel active area	$cm^2$
$a$	Channel width	$m$
$b$	Land width	$m$
$c$	Channel depth	$m$
$c_p$	Specific heat	$J\ kg^{-1}\ K^{-1}$
$D$	Diameter	$m$
$D_H$	Hydraulic diameter	$m$
$f_D$	Darcy friction factor	-
$k$	Thermal conductivity	$W\ m^{-1}\ K^{-1}$
$L$	Unfolded channel length	$m$
$\Delta P$	Pressure drop	$Pa$
$q$	Flow rate	$cm^3/min$
$Re$	Reynolds number	-
$v$	Velocity	$m/s$
$\rho$	Density	$kg/m^3$
$\mu$	Fluid viscosity	$Pa \cdot s$
$\emptyset$	Function of dissipation	-

# INTRODUCTION

Increased pollution, health risks associated with fossil fuel consumption, and rapid depletion of fossil fuel reserves have increased the importance of alternative energy supplies and promoted studies to focus on alternative energy-based power sources in recent years [1]. While wind, solar, and geothermal energy are marketed as carbon-neutral green energy sources, their reliance on natural conditions and limitations on application to mobile systems make them unpredictable and unreliable. Hydrogen fuel cell systems are considered to be one of the most effective applications for future energy generation. They are highly efficient in converting the chemical energy contained in the fuel into usable electricity. In 1839, a British scientist named William Grove became the first person to successfully construct a functional fuel cell. Fuel cells have a number of characteristics that make them particularly well-suited for energy production. When it comes to commercial applications, the proton exchange membrane fuel cell (PEMFC) is one of the most promising options for energy generation on the market. In terms of waste products, hydrogen fuel cells generate just heat and water, making them one of the most environmentally friendly methods of generating electricity. Because hydrogen fuel cells do not generate greenhouse gas emissions in the same way that fossil fuels do, this helps to reduce pollution and improve air quality. The use of hydrogen fuel cell technology provides a high-density source of energy with a high level of efficiency. The energy density of hydrogen is the highest of any conventional fuel. When compared to other forms of renewable energy, such as wind power, hydrogen fuel cells do not produce any noise pollution. Similarly to electric vehicles, hydrogen-fueled vehicles are substantially quieter than vehicles powered by internal combustion engines, which is a benefit for the environment. It is small and lightweight, and it responds quickly to power demands.

## INTRODUCTION

The type of electrolyte that a fuel cell utilizes is the fundamental property that distinguishes it from other types of cells. This classification dictates the types of electrochemical processes that take place in the cell, as well as the types of catalysts and fuels that are needed to carry out those operations. Types of fuel cells include Polymer electrolyte membrane (PEMFC), alkaline (AFC), phosphoric acid (PAFC), molten carbonate (MCFC) and solid oxide (SOFC). Because the PEMFC is more efficient and less complicated to construct than other types of fuel cells, it is the most widely used type of fuel cell. Moreover, due to its low operating temperature, the PEM Fuel cell seems to be the most appealing alternative for automotive applications [2]. As a matter of fact, the primary focus of this investigation is on PEM fuel cells. Further explanation of the primary components of PEM fuel cells, as well as the operation of these devices, will be provided in the next two subsections.

### 1. The Polymer Electrolyte Membrane Fuel Cell's Primary Components

Proton exchange membrane fuel cells, also known as polymer electrolyte membrane fuel cells, are usually found to have the following components. On both the cathode and anode sides, a membrane electrode assembly (MEA) as well as two bipolar plates (BPs) are installed (see Figure 1).

## INTRODUCTION

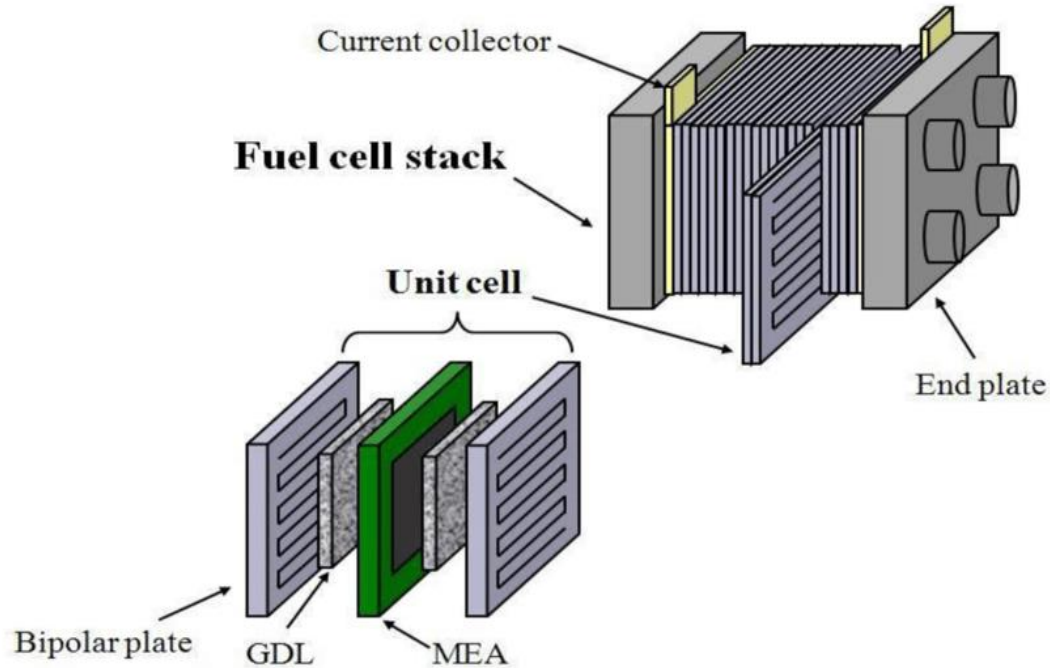


Figure 1. Design and fabrication of a PEM fuel cell stack [3].

### 1.1. Membrane Electrode Assembly (MEA)

PEM fuel cells cannot function without a membrane. Catalyst particles are doped into a polymer electrolyte membrane which is sandwiched between two electrodes to construct a fuel cell. As seen in Figure 2, a membrane electrode assembly is made up of an electrolyte, two gas diffusion layers, and two catalyst layers, with the electrolyte serving as the active layer.

The most widely utilized form of membrane material is Nafion<sup>®</sup>, which is a polymer membrane that belongs to the perfluorosulfonic acid (PFSA) family of polymers. The membrane's main jobs are to carry protons from one end of a cell to the other while blocking electrons from moving across it, and to separate the gases in nearby cells [4].

## INTRODUCTION

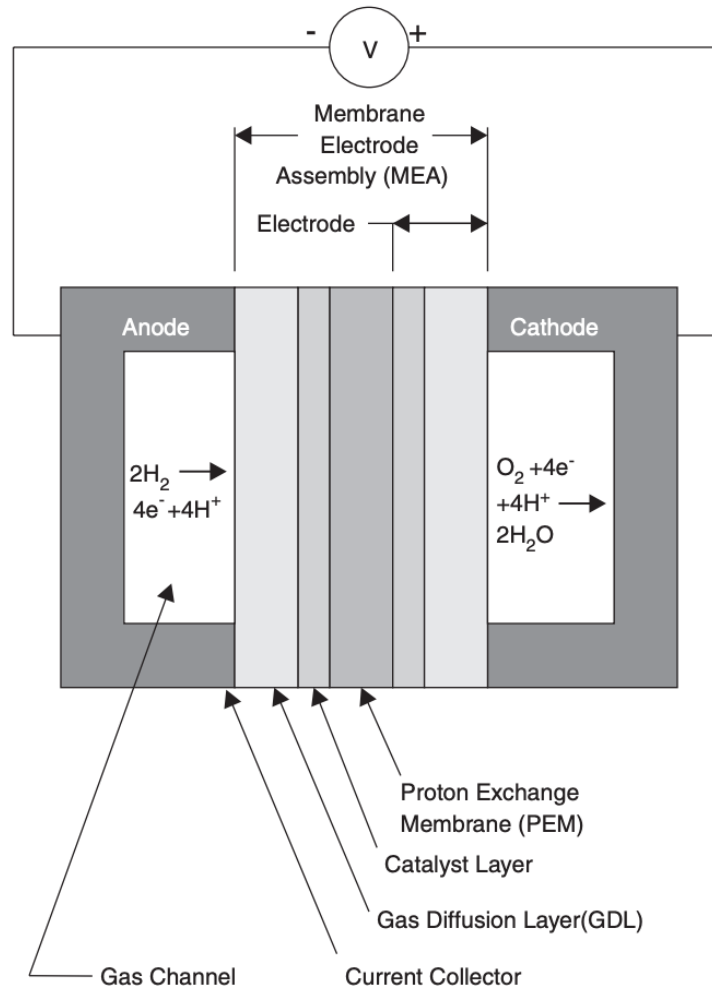


*Figure 2. Structure of a membrane electrode assembly [5].*

When it comes to PEM fuel cells, the catalyst layer has a sophisticated structure that includes both cathode and anode layers, allowing for half-electrochemical processes to take place. A fuel cell's anode is located on its negative side, and it is accountable for transferring the electrons that are freed during the hydrogen oxidation process to a separate circuit outside of the fuel cell, where they can be utilized to create electricity. The cathode is the positive side of the fuel cell, and it sends electrons from the exterior circuit to the catalyst, where they are used and mixed with hydrogen ions and oxygen to form water [6].

## INTRODUCTION

Between the catalyst layer and the bipolar plates lies the gas diffusion layer. It is constructed using spongelike materials such as carbon fiber or carbon fabric. Connecting the bipolar plate to the channel-land structure in a PEM fuel cell is one of the main jobs of the gas diffusion layer. The GDL acts as a conduit for reactants to go from channels to the catalyst layer while also assisting in the removal of by-product water from the catalyst layer in order to prevent flooding of the catalyst layer. Furthermore, it offers sufficient mechanical strength to prevent the membrane electrode assembly from expanding as a result of water absorption, as well as protection for the catalyst layer against corrosion or erosion induced by flows or by other external influences. The additional principal duties of the membrane are the transferring of heat during cell operation and the retention of a small amount of water on the surface to allow for conductivity through the membrane. [4].

### 1.2. Bipolar Plates

As a result of graphite's exceptional mechanical, electrical, and thermal properties, it has generally been used to make fuel cell bipolar plates (also known as flow field plates). The PEM fuel cell stack's bipolar plates account for around 80% of its weight and about 45% of its cost [7]. The bipolar plates of a PEM fuel cell are capable of carrying out a wide range of activities in a single cell. They are responsible for connecting and transporting electrons from the cell to an external wiring, separating the reactant gas in a neighboring cell, transferring heat from the active cell to the surroundings and to the stack's cooling unit, and providing structural support to the stack [4].

Channels on the bipolar plates make up the PEMFC's flow field and are responsible for transporting reactants to the reaction site efficiently and removing water from the fuel cell's periphery. It has been attempted to improve the performance of fuel

## INTRODUCTION

cells by experimenting with different flow field configurations. As a result of this understanding, flow field designs may be classified into three categories: fundamental, bio-inspired or nature-inspired, and hybrid.

### 1.2.1. Fundamental Flow Field Designs

The four most commonly used flow field configurations are depicted visually in Figure 3. They are referred to as conventional designs, and they include flow fields that are serpentine, parallel, pin-type, and interdigitated.

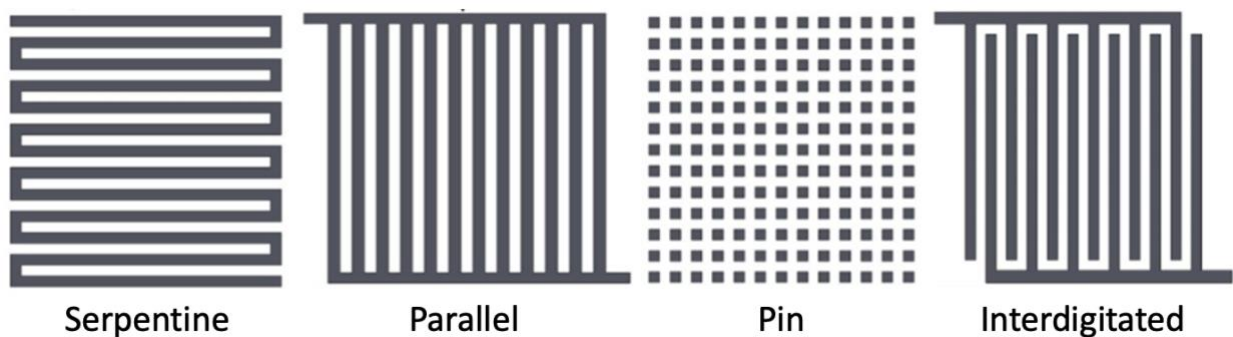


*Figure 3. The most common flow field designs used in PEMFCs.*

Serpentine designs have taken over as the industry model due to their greater performance [8]. They are frequently used as a benchmark for evaluating new designs. On the other hand, because of the high pressure needed to move gas from the inlet to the outlet, the principal disadvantages of this design are friction and channel narrowness. Parallel-serpentine hybrids with smaller cells and extra channels, as well as parallel-serpentine combinations, have all been developed to overcome this issue.

The pressure required to transfer gas through a parallel system is less than that required to move gas through a serpentine system since there are numerous parallel channels running from the input to the output. Because of the minimal pressure loss associated with parallel designs, the need for external blowers may be greatly

## INTRODUCTION

minimized [9]. However, water droplets may build up in the flow channels as a result of the low pressure. Because of the formation of these droplets, there is an uneven distribution of reactive gases throughout the channel, eventually clogging it. As a result, hot and cold patches have a detrimental influence on the overall performance and efficiency of the system. When it comes to overall performance, parallel structures are frequently the least efficient of the available options.

It has already been mentioned that water droplets might cause blockages in parallel design channels. In order to overcome this issue, there is one type of fundamental flow field design that can be treated as a particular form of parallel design called pin-type or mesh design channels, which creates a grid-like structure by leaving the routes between the parallel lines free [10]. Because of the massive volumes of water that are created as a result of using these systems for lengthy periods of time at high power consumption, flooding may occur as a result of their use. In certain modifications, metal meshes or sponges can be utilized to generate a variety of pathways from which to choose. Unfortunately, they will experience far more corrosion, which may result in premature cell failure.

The pathway from the inlet to the outlet in an interdigitated design is not consistent. Therefore, they contribute to the delivery of reactants to reaction spots as well as the removal of water from the diffusion medium. In general, interdigitated designs outperform parallel designs, but serpentine designs surpass both of them [11]. However, these are contingent on the working conditions. Water management in interdigitated designs appears to be superior to that of parallel designs, and they do this without the high pressure drops that are common in serpentine designs.

### 1.2.2. Nature-inspired Flow Field Designs

Nature-inspired flow field designs, on the other hand, have the potential to greatly increase the fuel cell performance by distributing reactant gases without suffocating them in water. There must be a delicate balance struck between a flow field's many variables, including gas distribution, flood control and electron transmission as well as pressure drop and manufacturing efficiency [8].

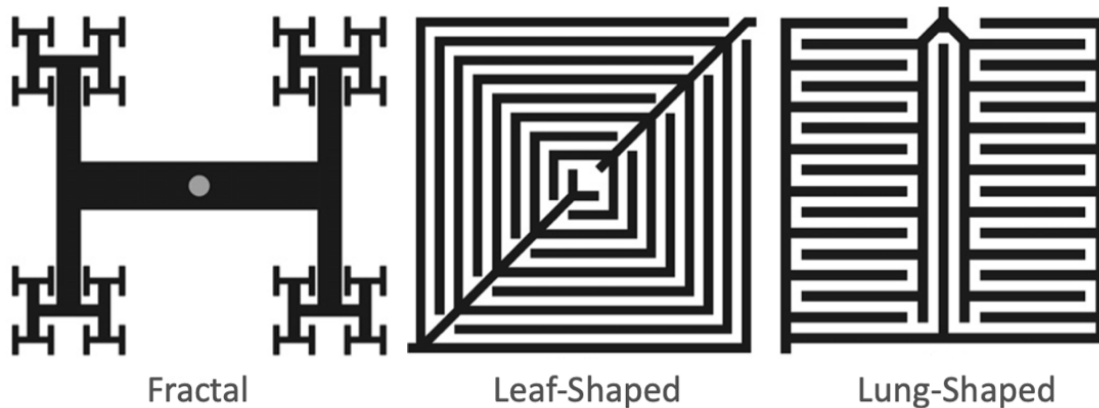


Figure 4. A representation of fractal and biological structures in schematic form [8].

Natural inspiration for the design of PEMFC flow fields comes from both fractal and biological sources (see Figure 4). In PEMFC fractal designs, self-similarity is emphasized with an emphasis on branching patterns at various scales. Animal and plant fluid transport systems, including leaves, arteries, lungs, and other organs, serve as inspiration for the bio or nature models.

### 1.2.3. Hybrid Flow Field Designs

Hybrid flow field designs, as the name indicates, are influenced by the combination of two separate design patterns in the search to improve performance and efficiency. The following are the most typical hybrid flow field design combinations: bio-inspired and interdigitated; bio-inspired and parallel. When it came to the channel

## INTRODUCTION

design approach, Murray's law was extensively employed in both circumstances to guide the decisions.

A biological structure's ability to transmit mass in the systemic circulation and sustain metabolic processes is derived from Murray's law, which is based on the smallest amount of energy necessary to do so. Murray's law states that the least degree of resistance to flow exists in a branching system, as is illustrated in Figure 5. A thorough description of Murray's law may be found in reference [12], which includes a formal derivation of the concept.

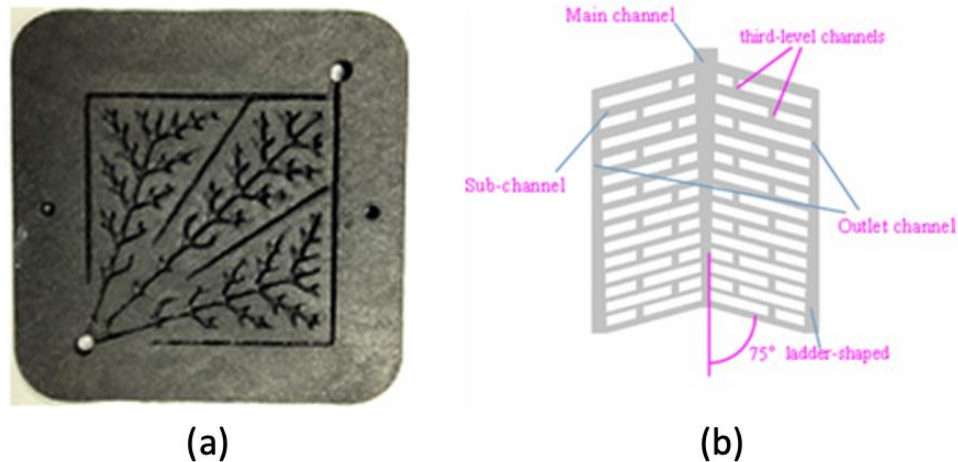


Figure 5. Hybrid flow field designs: (a) nature-inspired and interdigitated, (b) nature-inspired and parallel [13].

## 2. The PEM Fuel Cell's Fundamental Operation

For ions to move from one electrode to the next, an electrolyte connects the two electrodes (anode and cathode), and an external circuit allows current to pass between these electrodes. Fuel cells create protons ( $H^+$ ) and electrons ( $e^-$ ) when hydrogen combines with the anode catalyst layer. The cathode receives the protons as they flow through the membrane. For the anode-to-cathode transfer of electrons, an external

## INTRODUCTION

circuit is required. Oxygen serves as a reactive gas at the fuel cell's cathode. At the cathode, electrons and protons combine with oxygen molecules to produce water, which is subsequently expelled from the cell by the electrochemical reaction. A PEM fuel cell's transport methods are depicted in Figure 6.

Below is a breakdown of the electrochemical processes that take place within a PEM fuel cell. The following is what happens on the anode side of the reaction:



The following is the reaction that happens on the cathode side of the electrolyte:



Combining both the anode and cathode reactions into a single process results in the following:

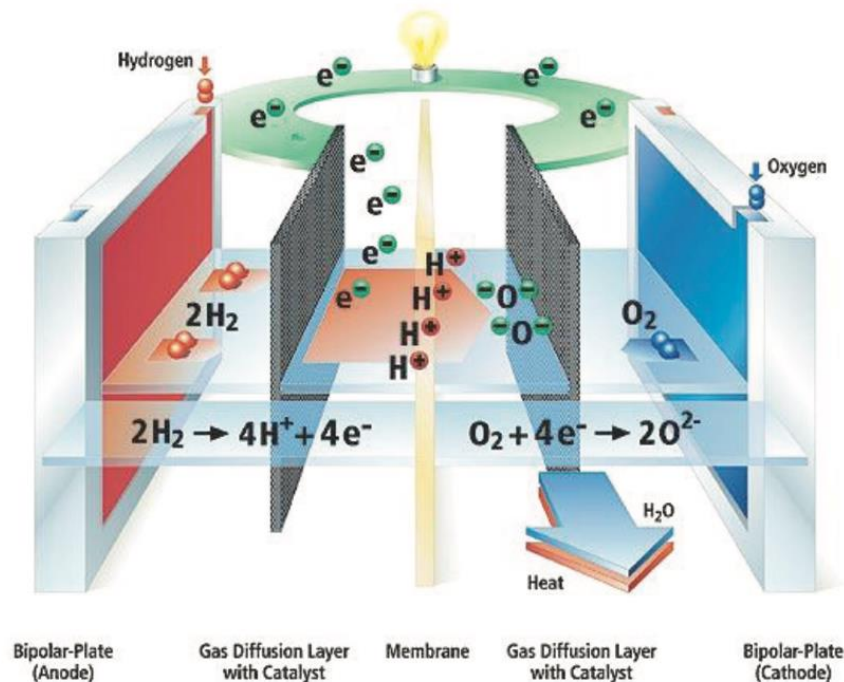


Figure 6. A PEM fuel cell's transportation procedure [14].

# LITERATURE REVIEW

Many academics are interested in fuel cell technology because of its environmentally-safe, cost-effective, and noise-free qualities. The field of fuel cell technology research encompasses a fairly broad range of topics. Among the topics covered are material research and manufacturing, fuel cell stack building (including performance analysis and testing), modeling and degradation, and any associated socio-economic and environmental issues. The majority of this study is devoted to the design of flow fields for bipolar plates, which is the primary objective. Therefore, the scope of my literature research will be confined to works on the flow field design of bipolar plate.

The bipolar plate and the arrangement of flow fields on the FC are two of the most remarkable features of the module. In addition to delivering compounds to the reaction site, bipolar plates are capable of removing unwanted products from the device. In order to achieve effective energy and mass transport, flow channels play an important role in the operation of the FC. The uniformity of reagent distribution and propagation through the cathode side is also helpful in achieving a uniform current density. As a result, the precise design of the flow field and the selection of an appropriate size are important to the proper operation of FCs. The flow field design of polymer electrolyte membrane fuel cells has been the subject of extensive research, which has either been completed or is still underway.

## 1. Fundamental designs

In fundamental designs, a range of different flow channel types and layouts have been introduced. Xianguo and Imran (2005) have conducted a thorough analysis of the advantages and disadvantages of various designs. It was discovered that humidity has

## LITERATURE REVIEW

an effect on the gas distribution in fuel cells by Dutta *et al.* (1999), who carried out a computational and experimental analysis. A considerable pressure drop was experienced on each bend of the serpentine design, and the current density generated was not uniform across the serpentine pattern. Brooks and Mina (2012) have offered an innovative and unique radial flow field design, and the results show that they've managed to boost performance while retaining a pressure drop that's less than half that of the serpentine flow field.

In their investigation, Watkins *et al.* (1991) looked into the issue of water floods caused by insufficient water removal. According to their design suggestion, an entry and an exit would be positioned at the opposite extremities of a serpentine flow field. To create zones of free flow, the reactant gases required to travel through the matching electrode's active area. At high current densities, a single water channel captures all liquid water produced by the electrode reaction site, decreasing the flooding effect. Using two different channel widths and two different flow-field topologies, Su *et al.* (2006) studied flooding difficulties in the cathode serpentine and serpentine-interdigitated flow fields.

To compare various flow channel configurations, Ming and Su (2007) used a three-dimensional CFD model. They discovered that a PEMFC with flow channels that vary step-wise in depth performs better than one with uniform depth channels. A serpentine flow channel's depth did not alter the FC's behavior. The model's predictions and trials clearly show that it can effectively aid with the optimal design of flow channels for the PEMFC. Straight parallel flow-fields were studied by Scholta *et al.* (2004) to determine the effect of channel size on flow-field geometry. According to a study evaluated by Hossain *et al.* (2017), both Z-type and U-type parallel channel topologies were examined to improve fuel cell flow uniformity and air dispersion in the parallel channel flow field.

## LITERATURE REVIEW

When it comes to pin-type flow field setups, Guo *et al.* (2013) investigated a network-based optimization approach. While optimizing, flow homogeneity was examined with and without taking into account reactant consumption in flow channels throughout the process. In three-dimensional numerical simulations, the new PEM fuel cell models were evaluated for their accuracy and efficiency. Both modified designs outperformed the standard pin-type structure in a fuel cell test by a wide margin. Seyed and Ebrahim (2019) came up with a new pattern called the "honeycomb flow field," which uses hexagonal pins in a regular grid arrangement.

Since the introduction of the interdigitated design for PEMFC flow patterns, it has proven to be more effective. The convective flow across the GDL is boosted by this flow design, resulting in a higher usage of the chemical components and an increased elimination of water. As a convenient reference for cell designers, Cooper *et al.* (2016) have conducted experiments with interdigitated and parallel flow field design parameters in order to give a useful resource.

## 2. Nature-inspired designs

Fuel cells with bio-inspired flow patterns have been studied for their impact on performance in several articles; while these new designs have improved in certain ways, they still fall short of fundamental designs. According to experimental studies by Tüber *et al.* (2004), transporting reactants from intake to exit may be accomplished using a fractal design that utilizes many parallel subdividing channels. Because of the numerous parallel channels and water blockage in these channels, their data showed that the fuel cell's performance was somewhat greater than the parallel but lower than the serpentine design. There are several bio-inspired flow field designs that were developed by Guo *et al.* (2014), and these were inspired by the venation structure found in tree leaves. By 20–25% compared to conventional designs, the bio-inspired interdigitated

## LITERATURE REVIEW

designs boost the performance of the fuel cells. An innovative bipolar plate design based on leaf fluid flow patterns is described and studied by Roshandel *et al.* (2012). According to the data, power density was marginally higher than in parallel and serpentine flow channels. Even while bio-inspired flow fields could potentially profit from the complex patterns of natural distribution systems, only a small number of these designs were able to achieve this goal.

### 3. Thesis Objective

The primary objective of this thesis is to investigate the fluid dynamics in the PEM fuel cell's bipolar plate flow channel when it is exposed to geometrical modifications. From the reviewed literature, serpentine channels have been shown to be the most promising fundamental flow field designs, and they have been utilized as the factory standard to assess other flow field designs. As a result, in this work, I intend to conduct both numerical (3D) and analytical analysis of the geometrical adjustments that have been made to the flow field channels. The performances of these configurations are compared to those of a serpentine flow field design that has been obtained from the literature to provide a baseline for comparison. The pressure drop between the flow field inlet and outlet is a good indicator of the applicability of new modifications to flow field channels.

## THEORY AND MODELLING

### 1. Analytical Analysis

There are three types of flow in a pipe: laminar flow, turbulent flow, and although it is generally not preferred to stay in that region, there is transition as well. It was a British physicist and mathematician named Osborne Reynolds (1842–1912) who used a simple device to discern between the two types of flows. The Reynolds number,  $Re$ , which measures the flow's inertia to viscosity, is the most critical dimensionless parameter for pipe flow. If the Reynolds number is "little enough," "middle," or "big enough," the flow in a pipe is either laminar, transitional, or turbulent. Although the fluid velocity is important, other factors such as density, viscosity, and pipe size also have an impact on the flow's characteristics. The Reynolds number is the result of the combination of these parameters. It was not until 1883 that Osborne Reynolds discovered that laminar and turbulent pipe flow can be distinguished by a suitable dimensionless quantity.

$$Re = \frac{\rho v D}{\mu} \quad (4)$$

where  $\rho$  is density,  $v$  is velocity,  $D$  is pipe diameter and  $\mu$  is fluid viscosity.

Now it's time to think about how we can tell the difference between laminar and turbulent pipe flow. The presence of laminar flow in a round pipe occurs when the Reynolds number is less than approximately 2100. In a round pipe, when the Reynolds number exceeds approximately 4000, the flow is considered turbulent. It is possible that the flow will oscillate between laminar and turbulent phases in an almost random manner between these two constraints (transitional flow).

The cross section of all of the flow channels that were designed for this investigation is rectangular. In the context of flow in noncircular tubes and channels, the term "hydraulic diameter ( $D_H$ )" is almost certainly familiar. This phrase can be used

## THEORY AND MODELLING

to perform a variety of calculations in the same way that they would be performed for a round tube. The following formula should be used in order to get the hydraulic diameter of a rectangular duct:

$$D_H = \frac{2ac}{a + c} \quad (5)$$

where  $a$  and  $c$  are the length of the sides of a rectangular tube.

We will therefore substitute hydraulic diameter( $D_H$ ) for pipe diameter( $D$ ) in equation 4 for the purpose of calculating the Reynolds number.

In most circumstances, analytical calculations are required in addition to numerical simulations in order to validate numerical findings with properly derived conclusions from theory. A PEMFC's flow channels in the bipolar plates are typically tested using pressure drop to see how well they work. This is because the channel's entrance and outlet have different pressures, which causes the fluid to flow. The pressure drop between the input and output can be raised to improve fluid velocity. However, because of the increased pressure drop, there may be large pressure differences along the fuel channel. To put it another way, this means that the fuel is being dispersed to the MEA layers at different pressures over the cell surface area.

When reactant gases move through the cell, friction within the passages causes a pressure drop ( $\Delta P$ ). Equation 7 can be used to calculate the flow rate-pressure drop relationships for uniform, non-compressible pipe flows and it is known as the Darcy-Weisbach Equation. When solving the Darcy-Weisbach equation, a non-dimensional friction factor known as the Darcy friction factor ( $f_D$ ) must be taken into consideration, and it is inversely proportional to the Reynolds Number in laminar flow regime. Friction factor for pipes with square cross section is following:

$$f_D = \frac{56}{Re} \quad (6)$$

$$\Delta P = \frac{f_D \rho v^2 L}{2D_H} \quad (7)$$

where  $\rho$  is density,  $v$  is velocity,  $D_H$  is hydraulic diameter and  $L$  is unfolded channel length.

## 2. Governing Equations

The dynamics of fluid flow are governed by Navier - Stokes equations that describe mass, momentum, and energy conservation. As can be seen from the flow variables' time and space evolution, these equations reflect the interaction between the flow parameters and their propagation in time and space.

In this case, consider a generic flow field and the probability of a closed volume drowning within a limited part of the flow stream. In order to regulate the volume, we may construct a control volume (V) and a control surface (S), which is a closed surface that defines the volume's boundaries . A fixed control volume in space may be used in conjunction with fluid flowing through it. This means that fundamental physical rules are employed to both regulate volume fluids as well as control surface fluids [15]. Now one can discuss how to derive the integral versions of the fluid flow equations by applying the basic physical principles to a limited control volume and directly getting them. By altering the integral forms of the Navier - Stokes equations, it is possible to obtain partial differential equations without having to solve them directly in the traditional way.

## 2.1. Continuity Equation

The overall rate of mass flux out of  $V$  must equal the rate of mass decrease inside the control volume  $V$ , and the partial differential form is shown in the following equation:

$$\frac{\partial \rho}{\partial t} + \frac{\partial(\rho u)}{\partial x} + \frac{\partial(\rho v)}{\partial y} + \frac{\partial(\rho w)}{\partial z} = 0 \quad (8)$$

where  $\rho$  is the fluid density,  $(u, v, w)$  are the velocity components in  $(x, y, z)$  direction, respectively.

## 2.2. Momentum Equation

There must be an equal and opposite relationship between the element's rate of change of momentum and the element's net force. The conservation of momentum equation can be expressed as follows:

Momentum ( $x$ -direction):

$$\rho \left( \frac{\partial u}{\partial t} + u \frac{\partial u}{\partial x} + v \frac{\partial u}{\partial y} + w \frac{\partial u}{\partial z} \right) = -\frac{\partial p}{\partial x} + \mu \left( \frac{\partial^2 u}{\partial x^2} + \frac{\partial^2 u}{\partial y^2} + \frac{\partial^2 u}{\partial z^2} \right) \quad (9)$$

Momentum ( $y$ -direction):

$$\rho \left( \frac{\partial v}{\partial t} + u \frac{\partial v}{\partial x} + v \frac{\partial v}{\partial y} + w \frac{\partial v}{\partial z} \right) = -\frac{\partial p}{\partial y} + \mu \left( \frac{\partial^2 v}{\partial x^2} + \frac{\partial^2 v}{\partial y^2} + \frac{\partial^2 v}{\partial z^2} \right) \quad (10)$$

Momentum ( $z$ -direction):

$$\rho \left( \frac{\partial w}{\partial t} + u \frac{\partial w}{\partial x} + v \frac{\partial w}{\partial y} + w \frac{\partial w}{\partial z} \right) = -\frac{\partial p}{\partial z} + \mu \left( \frac{\partial^2 w}{\partial x^2} + \frac{\partial^2 w}{\partial y^2} + \frac{\partial^2 w}{\partial z^2} \right) \quad (11)$$

where  $\mu$  is the viscosity of the fluid in the channel.

Momentum changes cause the terms on the left to be referred to as "inertial terms." In all of these cases, resistance is provided by the pressure profile as well as by viscous forces, which operate to suffocate the flow at all times, as well as by body forces when present. The velocity of a single fluid element may be quantified over time by

referring to it as inertial. The temporal derivative, also known as the local derivative, provides information about the change in velocity at a particular point. An analysis under steady-state conditions will eliminate these temporal terms from the equation. They are known as convective terms, and they comprise the last three inertial terms.

### 2.3. Energy Equation

The rate at which energy moves in and out of the fluid element must be the same as the rate at which work is done on it by body and surface forces. Using Newtonian fluids and incompressible flow as assumptions, the equation can be expressed as follows:

$$\begin{aligned} \rho c_p \left( \frac{\partial T}{\partial t} + u \frac{\partial T}{\partial x} + v \frac{\partial T}{\partial y} + w \frac{\partial T}{\partial z} \right) \\ = \frac{\partial}{\partial x} \left( k \frac{\partial T}{\partial x} \right) + \frac{\partial}{\partial y} \left( k \frac{\partial T}{\partial y} \right) + \frac{\partial}{\partial z} \left( k \frac{\partial T}{\partial z} \right) + \phi \quad (12) \\ + \left( u \frac{\partial p}{\partial x} + v \frac{\partial p}{\partial y} + w \frac{\partial p}{\partial z} \right) \end{aligned}$$

where  $c_p$  is the specific heat at constant pressure,  $k$  is the thermal conductivity,  $\phi$  is the function of dissipation.

When dealing with all of the governing equations, it is necessary to give the energy equation. Due to the fact that this research will only be concerned with the flow field for isothermal studies, the energy equation will not be solved in this study.

## 3. Model Development

The low cost and quick turnaround time of computer simulations make them an excellent tool for testing PEMFC flow field design. Computational fluid dynamics (CFD) modeling is frequently used in the creation of PEMFC simulations.

### 3.1. Simulation Technique

For the sake of simulating the outcomes of this work, ANSYS® 2019 R3 engineering simulation program and SOLIDWORKS® 3D CAD design tools were utilized. The instructions for performing simulation activities are laid out in a logical sequence, with each step leading to the next.

The generation of a valid and reliable model is the first step in obtaining more accurate results in the final step, and it is the most important. Due to the fact that it incorporates basic sketch parameters for 2D design as well as crucial features for converting 2D sketches into 3D models, SolidWorks is a powerful geometry tool. Furthermore, these models may be simply imported into a variety of simulation software packages. Before importing the solid model into the CFD environment, it is necessary to identify and correct any issues within the model.

The meshing stage of computational fluid dynamics (CFD) is time-consuming and labor-intensive, yet it is crucial to the accuracy of the solution. Imported solid models can be meshed in a variety of ways using the ANSYS Workbench meshing tool. Following the creation of a working mesh, it is possible to perform quality metrics on it and make iterations until a desirable level of quality satisfaction is reached.

Last but not least, the fluid phenomena in flow channels can be modelled using the FLUENT software. An integrated post-processing feature makes it simple to halt and evaluate results while ANSYS FLUENT's interactive solver sets up, solves, and then resumes the calculation. When it comes to modeling, the solution parameters include three-dimensional, double precision, and serial processing. The algorithm of SIMPLE method is used to solve the coupled equations for velocity and pressure. As this thesis progresses, additional information will be supplied about the particular research case that was examined in this work.

### 3.2. Mesh

An accurate simulation is dependent on the precision of its mesh, which is one of the most critical factors to consider. A numerical solution of the Navier-Stokes equations is performed at each mesh element in order to approximate the process at each point in the domain, and this is done using a variety of approaches. Each of these methods is selected according to the complexity of the flow and whether the flow is laminar, turbulent, or both in 2D or 3D. The domain is reduced to a succession of smaller units by the use of the meshing process. Mesh independency investigations are required to confirm that the results of a CFD simulation are accurate regardless of the mesh size or element type used. It is possible to customize the meshing engine in ANSYS Workbench by adjusting its settings, which include changing its size and the types of grid components that are employed.

#### 3.2.1. Mesh Independence Study

Mesh independence is a term used to describe when a mesh is optimized to contain the lowest number of cells possible while the acquired solution remains unchanged regardless of how much mesh refining is performed. One common method of accomplishing this is to keep an eye on a fluid flow characteristic of interest as the grid becomes smaller and smaller. This could be the case for either the velocity or the pressure. In order to achieve the best possible results, at least three different grid resolutions have to be examined, with each succeeding mesh being either finer or coarser than the one before. When the grid cells are refined, the size of the grid cells is reduced while the number of cells in the flow domain is increased.

It is critical to start with a simple geometry or a crucial piece of a complicated geometry when performing mesh independence studies because this will result in fewer computing times and resources. The simple shape chosen for this analysis is a single

## THEORY AND MODELLING

serpentine channel with sharp corners, as illustrated in Figure 10. Until the very first corner, the channel is 40 mm long. It's at the depth of 1.5 mm, the width of the channel is 1 mm, and the angle at each corner is 90 degrees.

Simulations were carried out in order to investigate the relationship between the results of the pressure drop and the values of the total number of mesh elements in the geometry. To put it another way, the boundary constraints that were applied for the mesh independence analysis were the same for all of the simulated instances. The operating pressure and temperature were fixed at 2 atmospheres and 350 K, respectively, to ensure proper operation. The inlet velocity of the hydrogen gas was maintained at 10 cm<sup>3</sup>/s throughout the analysis. The only variable that changed across all of these simulations was the size of the mesh elements. Using 11 different mesh element sizes ranging from 0.1 to 0.6, of which only 3 distinctive mesh sizes are shown in Figure 8 for the sake of simplicity. As demonstrated in Table 1, the findings of the mesh independence investigation were found to be statistically significant. In addition, Figure 7 provides a graphical representation of the data.

*Table 1. Results of the mesh independence study.*

<b>#</b>	<b>Mesh Size [mm]</b>	<b>Number of Nodes</b>	<b>Number of Elements</b>	<b>Pressure Drop [Pa]</b>	<b>Error [%]</b>
1	0.1	5,545,131	1,228,500	978.40	5.2
2	0.15	1,718,804	359,010	947.24	8.3
3	0.2	823,242	163,800	912.19	11.7
4	0.25	419,421	78,624	861.05	16.6
5	0.3	264,398	47,390	815.15	21.1
6	0.35	165,978	28,044	764.63	25.9

## THEORY AND MODELLING

<b>#</b>	<b>Mesh Size [mm]</b>	<b>Number of Nodes</b>	<b>Number of Elements</b>	<b>Pressure Drop [Pa]</b>	<b>Error [%]</b>
7	0.4	128,003	20,848	720.41	30.3
8	0.45	87,986	13,572	680.84	34.1
9	0.5	67,187	9,828	636.97	38.3
10	0.55	61,447	8,988	638.04	38.2
11	0.6	47,342	6,453	569.06	44.9

The geometry was meshed in order to determine the most reasonable mesh by comparing the pressure drop value to the number of mesh cells in the geometry. Hexahedral elements were used to mesh the computational domain in all simulations.

The data in Table 1 clearly shows that the pressure drop value from the fourth mesh to the eleventh mesh differs significantly from the analytical pressure drop value by simply having a look at the errors. The differences in pressure drop values between the analytical pressure drop value and the pressure drop value derived from the first and second mesh values are 5 % and 8 %, respectively, according to the results. In this scenario, it would be rational to choose the first mesh because it has a smaller error than the second.

## THEORY AND MODELLING

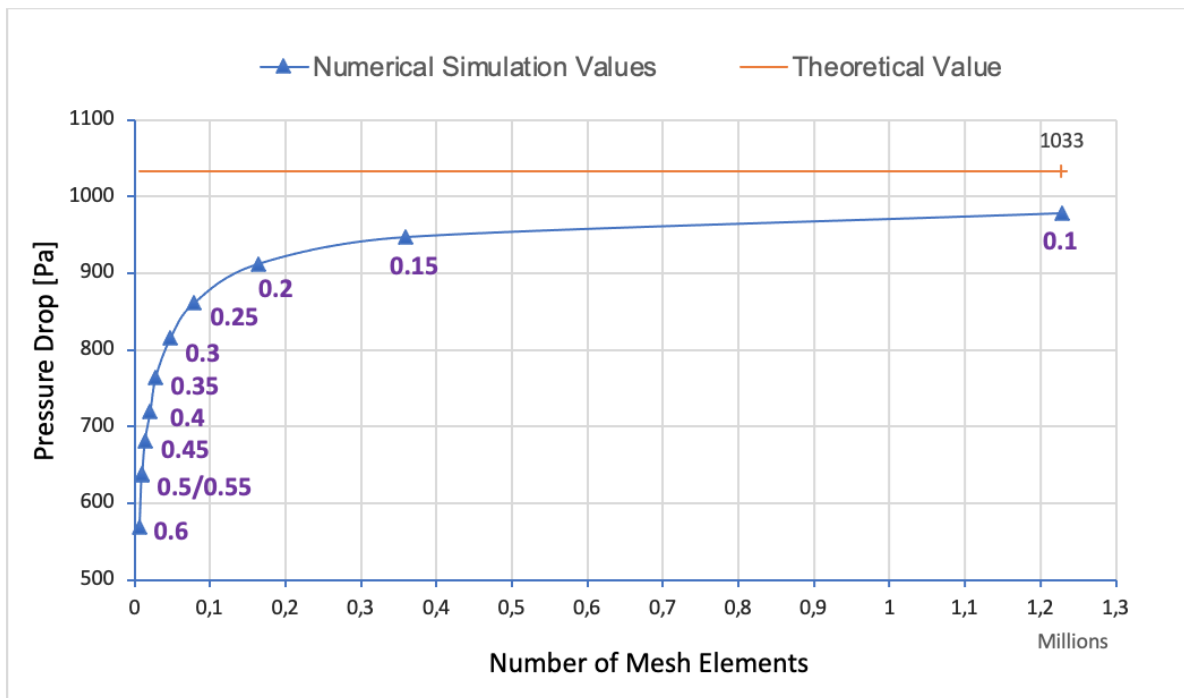


Figure 7. Graphical representation of mesh independence study.

However, there are several critical elements that must be taken into account, such as computing time and available resources. Larger elements produce poor results, while smaller elements prolong the computing process to the point where the results are not obtained at all. It is critical to strike a balance between computation time and accuracy when carrying out a mesh independence study. When you look at the first mesh, you will notice that the domain is divided into 1.2 million cells, despite the fact that the geometry chosen is the simplest. It is possible that the findings of the simulations would not have been obtained if the first mesh had been used for the other complex geometries. As a result, for the first mesh, there is no correlation between calculation time and accuracy.

## THEORY AND MODELLING

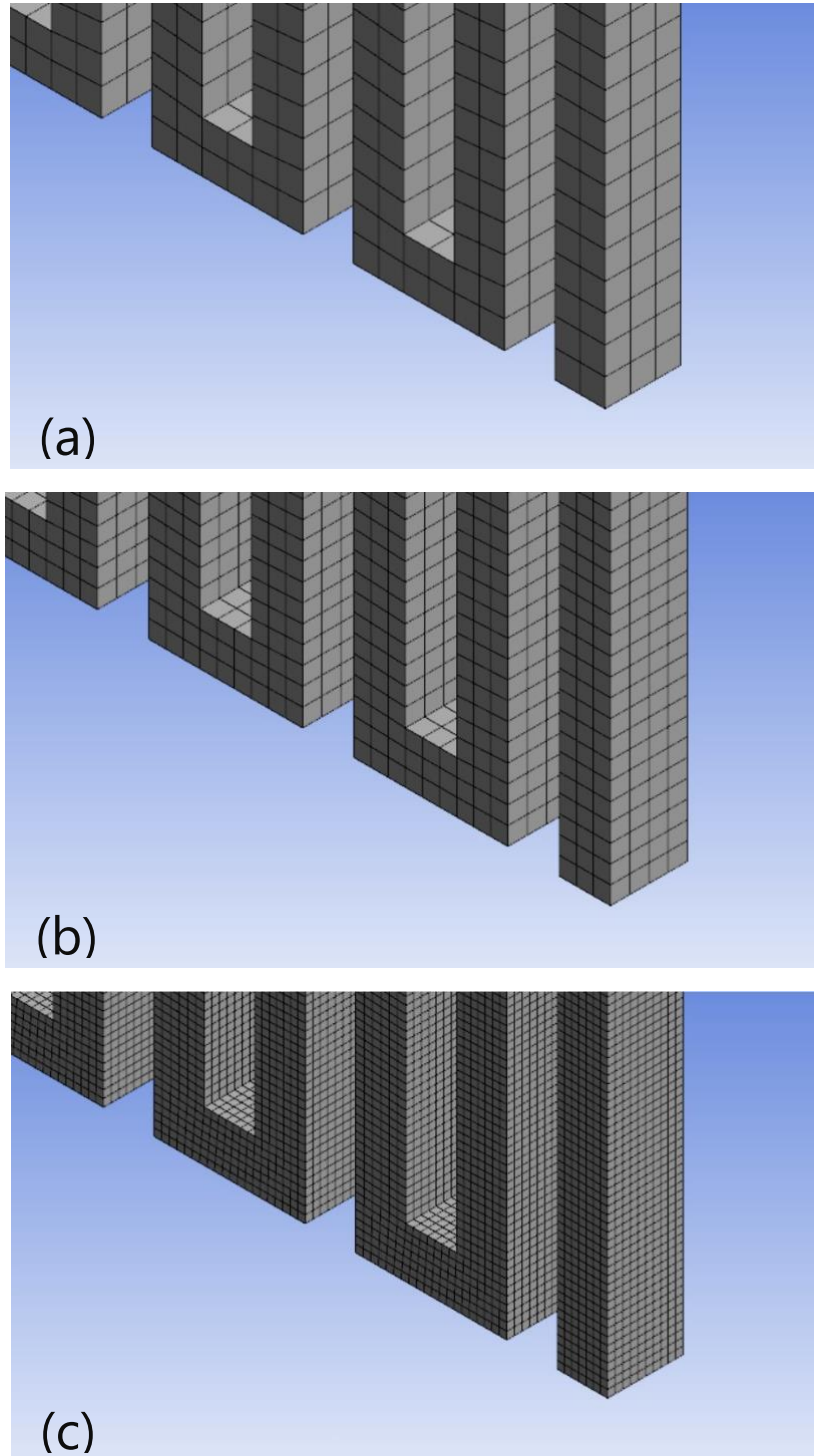


Figure 8. A portion of meshed geometry: (a) mesh size: 0.55, (b) mesh size: 0.35, (c) mesh size: 0.15

## THEORY AND MODELLING

Only 3.1 percent change in pressure drop was found between the first and second meshes, indicating that there was very little variance between the first and second meshes. The only other thing to point out is that there is only around an 8% difference between the analytical pressure drop value and the second mesh pressure drop result, which is a comparatively minor inaccuracy. It is reasonable to conclude that the second mesh result is sufficiently accurate to be taken into consideration in light of the foregoing. If we look at the computation time, the second mesh has 0.36 million cells, which is substantially fewer than that of the first mesh, allowing for results to be produced in a reasonable amount of time even for complex geometries to be obtained. Consequently, in order to save time during the subsequent analysis, the second mesh with an element size of 0.15 mm was chosen in the meantime, which is given in Figure 8.

During the meshing procedure in this research, the inflation option was not taken into consideration. To support this course of action, there are three primary justifications available.

In the first place, when compared to the pressure drop value resulting from the analytical analysis, the pressure drop value from the chosen mesh, which was established by the mesh independence study, has just an eight percent error. This suggests that the overall number of mesh elements generated during the meshing process is exceptionally sufficient to capture the flow behavior along the wall, especially at the corners of the channel.

## THEORY AND MODELLING

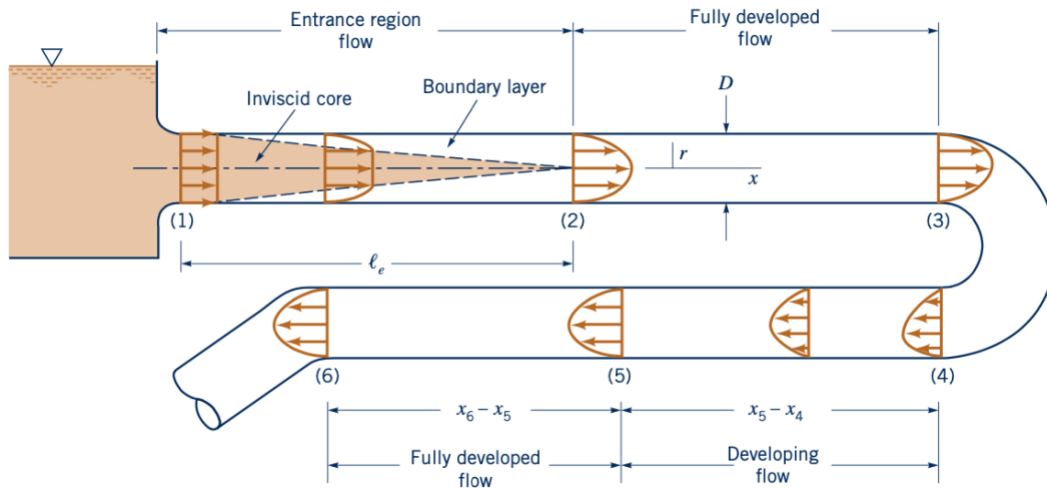


*Figure 9. Entrance region and fully developed flow. [16]*

Second, when the geometry is exceedingly complex and the mesh is unstructured, the inflating option can be extremely useful. However, in this study, all of the geometries have a structured mesh [17].

Last but not least, in a pipe, if the flow is fully developed until the first corner, then the velocity profile remains unchanged, as it is resembled in Figure 9. The primary reason behind selecting the inflation option is to capture the velocity profile in the wall boundary layer [16]. So, aside from the fact that the Reynolds numbers of all of the geometries in this study are extremely low, as shown in Table 6 and Table 8, it is necessary to determine the length of the entrance region in order to demonstrate that the flow is fully developed. In the analytical background chapter, it is discovered that the flow inside the channel is laminar. The following formula can be used to determine the length of the entrance region for laminar flow:

$$L_{e,laminar} = 0.0575Re \cdot D_H \quad (13)$$

where  $Re$  is Reynolds number,  $D_H$  is hydraulic diameter and  $L_{e,laminar}$  is length of the entrance region for laminar flow.

It is now necessary to compute the entrance length for the worst-case scenario for the geometry that was used for the mesh independence study. With the use of the provided formula, it is identified that the entrance length is equivalent to 2.32 cm. According to the geometry utilized, the length of the channel to the first corner is 4 cm, as illustrated in Figure 10. By comparing these two figures, it is possible to conclude that the flow within the channel is fully developed. Simply by taking into account all of the previously stated reasons, the notion of not using the inflation option during the meshing process is supported.

### 3.3. Serpentine Channel with Active Area of 4x4 cm<sup>2</sup>

The appropriate reference case's geometry is shown in the Figure 10. For the sake of simplicity, the effects of electrochemical processes are ignored in this study. A rectangular single-path serpentine shape was used as a starting point for the flow field design. After the simulation results were checked with analytical values, some modifications were made in order to reduce pressure drop. To assist in distinguishing this particular design from others, we will refer to it as a "4x4" simply because of the proportions of the necessary flow channels.

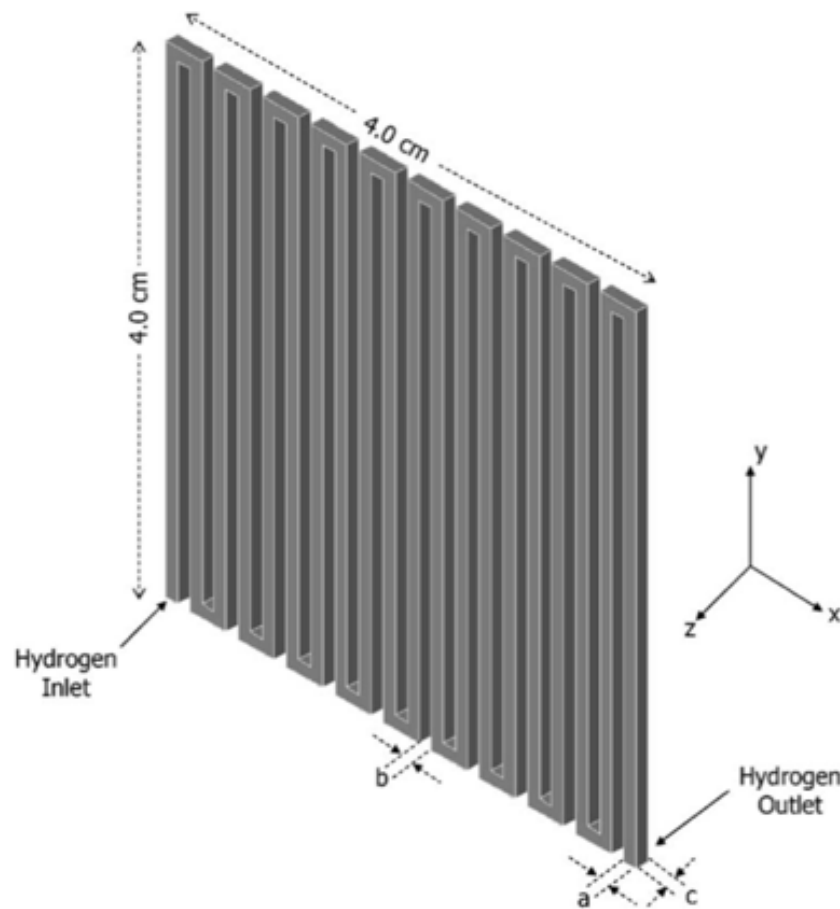


Figure 10. "4x4" Serpentine flow-field design in a bipolar plate. [10]

### 3.3.1. Problem Domain

Data from the geometry configuration are summarized in Table 2, which includes typical PEMFC flow field channel width, channel depth, and land width characteristics. Two modifications will be made to the "4x4" serpentine flow field in order to see results. There is no doubt that sharp edges are to blame for the increased pressure drop in literature review. First, the flow field channel turns will have their sharp edges replaced with obvious curvatures as a result of this new finding. The second change will be to add an extra inlet, as shown in the Figure 11. To make reliable statements about the

value of the pressure drop, these two cases will have the identical channel area and dimensions.

Table 2. Primary dimensions for the "4x4" model.

Characteristics	Sizing
Channel area [cm <sup>2</sup> ]	4 x 4
Channel depth [mm]	1.5
Channel width [mm]	1
Land width [mm]	1

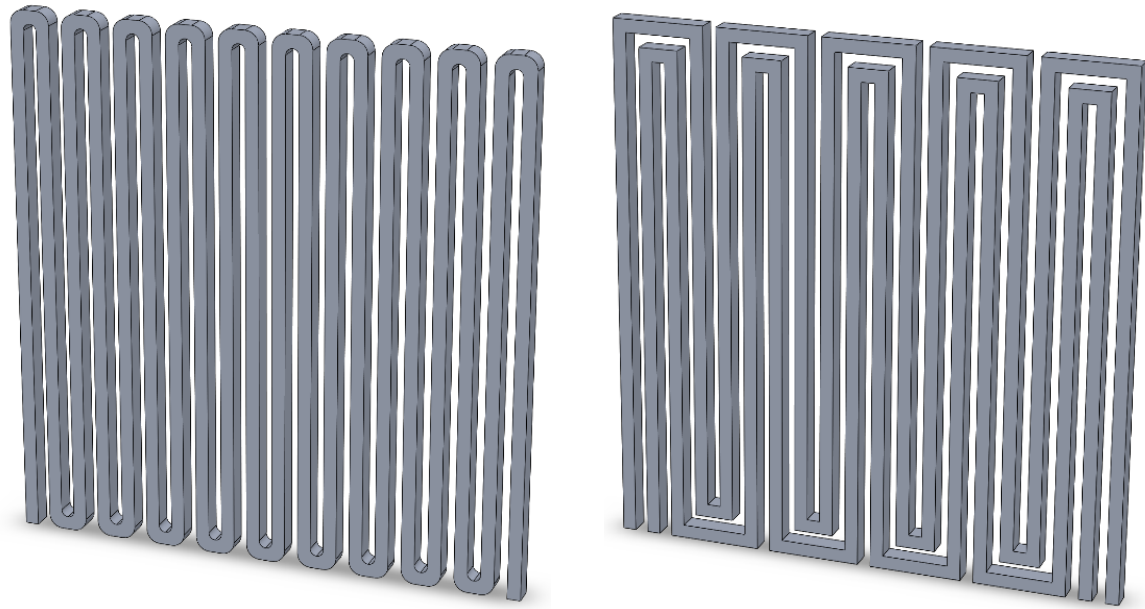


Figure 11. "4x4" model: Curvature (left) and Double inlet (right)

### 3.3.2. Model Assumptions

Given the current "4x4" three-dimensional numerical model's assumptions, the system runs under steady-state circumstances, and the influence of gravity is not taken into consideration at all. Isothermal conditions are expected to exist throughout the entire domain. Using Table 6, we can see that the Reynolds number ranges from 67 to

336, with the minimum being 67 and the maximum being 336. Due to the fact that the reported values are less than 2100, the flow inside the channel is laminar, which is consistent with the analytical analysis. The working fluid is considered to be hydrogen gas and operates according to the ideal gas law.

### 3.3.3. Boundary Conditions

The "4x4" model was subjected to the same boundary constraints, regardless of its geometrical configuration. In order to determine how the software will identify between the models, the borders of the model are useful information. It is useful to specify the flow rate in order to determine the Velocity Inlet boundary conditions, which is the first stage. An outlet with zero gauge pressure simulates a disposal into the atmosphere, and static operating pressure is employed for the Pressure Outlet boundary condition. Finally, for the Wall boundary condition, a constant temperature criterion as well as a non-slip condition are imposed. The boundaries that have been established for each component of the surface are listed in the following Table 3.

Table 3. Boundary conditions for the "4x4" model and for its modifications.

Boundary Conditions		Value
<b>Inlet</b>	Gas fuel inlet [cm <sup>3</sup> /s]	10-50
<b>Outlet</b>	Operating pressure [atm]	2
<b>Wall</b>	Temperature [K]	350

### 3.4. Serpentine Channel with Active Area of 10x10 cm<sup>2</sup>

The Figure 12 depicts the geometry of a suitable reference instance for our purposes. In this scenario, a rectangular single-path serpentine flow field on a bipolar

## THEORY AND MODELLING

plate with a bigger active area will be simulated. Once this is confirmed with Nattawut and Yottana (2011)'s case, the results will be considered accurate. Nevertheless, there was a shortage of data in the cited study. No specifics were provided as to the type of working fluid that had been simulated. First, the working fluid will be explored, and then the effect of a larger active area will be examined. In order to make things as basic as possible, electrochemical reactions have been excluded from the scope of this inquiry. In this particular design, the term "10x10" refers to the dimensions of the flow channels that are necessary, which helps to identify it from other designs.

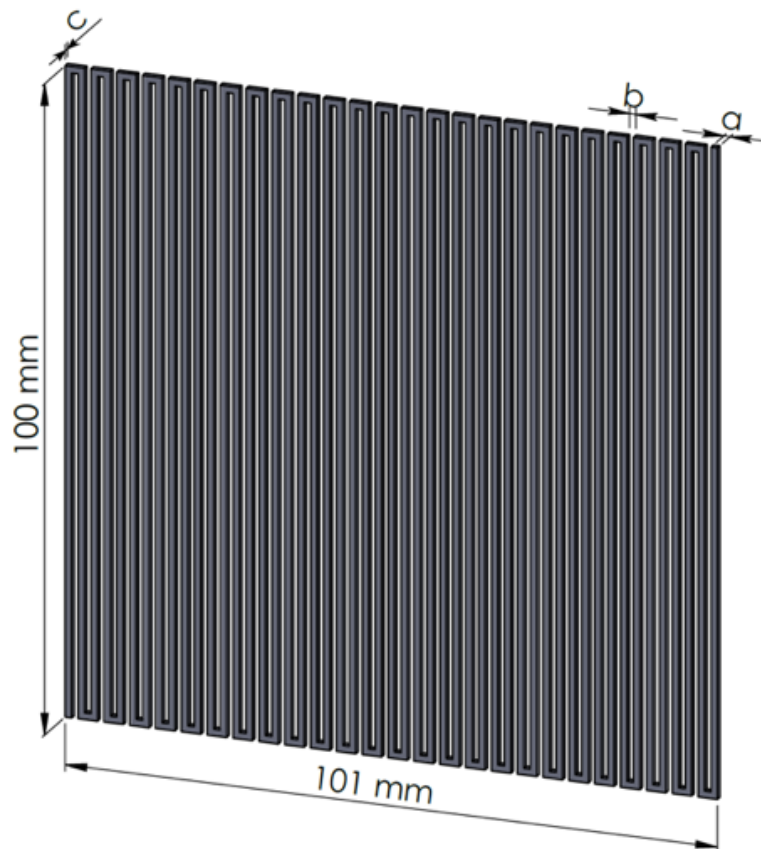


Figure 12. "10x10" Serpentine flow-field design in a bipolar plate. [14]

### 3.4.1. Problem Domain

The information from the geometry configuration is displayed in a Table 4 that contains conventional PEMFC flow field properties, such as the width of the flow field channel, its depth, and the breadth of the land surface.

Table 4. Primary dimensions for the "10x10" model.

Characteristics	Sizing
Channel area [cm <sup>2</sup> ]	10 x10
Channel depth [mm]	1
Channel width [mm]	1
Land width [mm]	1

### 3.4.2. Model Assumptions

The present "10x10" three-dimensional numerical model, which operates under steady-state conditions, does not take into consideration the effects of gravity at all. It is envisaged that isothermal conditions will prevail across the whole domain. Using Table 8, we can see that the Reynolds number ranges from 182 to 455, with the minimum being 182 and the maximum being 455. Due to the fact that the reported values are less than 2100, the flow inside the channel is laminar, which is consistent with the analytical analysis. A thorough analysis revealed that the working fluid was oxygen gas.

### 3.4.3. Boundary Conditions

The "10x10" model was subjected to the boundary constraints. In order to determine how the software will identify between the models, the borders of the model

## THEORY AND MODELLING

are useful information. It is useful to specify the flow rate in order to determine the Velocity Inlet boundary conditions, which is the first stage. An outlet with zero gauge pressure simulates a disposal into the atmosphere, and static operating pressure is employed for the Pressure Outlet boundary condition. Finally, for the Wall boundary condition, a constant temperature criterion as well as a non-slip condition are imposed. The boundaries that have been established for each component of the surface are listed in the following Table 5.

Table 5. Boundary conditions for "10x10" model.

Boundary Conditions		Value
<b>Inlet</b>	Gas fuel inlet [cm <sup>3</sup> /min]	200-500
<b>Outlet</b>	Operating pressure [atm]	1
<b>Wall</b>	Temperature [K]	323

## RESULTS AND DISCUSSION

### 1. Analytical Validation

It is planned to compute the Reynolds number with the help of analytical background information in order to determine whether the flow inside the flow channel is laminar or turbulent for the purpose of determining what actions should be taken in the future. Furthermore, after validating the Reynolds number, it is necessary to compute the hydraulic diameter because the cross section of all of the flow channels that were created for this inquiry has a rectangular cross section. The following step is to determine the Darcy friction factor. Using equation 7, it is possible to compute the pressure drop as a final step after gathering all of the necessary input data. The computed pressure drop value will be utilized to validate the numerical simulation findings in the numerical validation section, which will be covered in more detail later.

#### 1.1. Serpentine Channel with Active Area of 4x4 cm<sup>2</sup>

As previously stated, for noncircular tubes, the hydraulic diameter is computed and is shown in Table 7. The Reynolds number for each flow rate is provided in Table 6 by utilizing the relevant analysis parameters. In accordance with the information provided in the analytical background, it is conclusively demonstrated that the fluid within the flow channel is laminar because all values of the Reynolds number are significantly less than 2100.

*Table 6. Reynolds Number for "4x4" model.*

<i>Flow rate [m/s]</i>	6.66	13.33	20	26.66	33.33
<i>Reynolds number</i>	67.28	134.56	201.84	269.12	336.40

## RESULTS AND DISCUSSION

*Table 7. Necessary Analysis Parameters for "4x4" model.*

Parameters name	Value
H <sub>2</sub> viscosity @350K [ $\mu$ ]	0.9737x10 <sup>-5</sup> [Pa/s]
H <sub>2</sub> density [ $\rho$ ]	0.08189 [kg/m <sup>3</sup> ]
Hydraulic Diameter [ $D_H$ ]	0.0012 [m]
Unfolded channel length [ $L$ ]	0.819 [m]

### 1.2. Serpentine Channel with Active Area of 10x10 cm<sup>2</sup>

It is possible to compute the Reynolds number along the channel for any velocity variation by utilizing the analytical parameters listed in Table 9. As a result of the Reynolds number being less than 2100, Table 8 clearly demonstrates that the fluid in the flow channel is laminar, which is consistent with the analytical background provided.

*Table 8. Reynolds Number for "10x10" model.*

<i>Flow rate [m/s]</i>	3.33	5	6.66	8.33
<i>Reynolds number</i>	182.11	273.16	364.22	455.27

*Table 9. Necessary Analysis Parameters for "10x10" model.*

Oxygen properties	Value
Viscosity @323K [ $\mu$ ]	2.18x10 <sup>-5</sup> [Pa/s]
O <sub>2</sub> density [ $\rho$ ]	1.191 [kg/m <sup>3</sup> ]
Hydraulic Diameter [ $D_H$ ]	0.001 [m]
Unfolded channel length [ $L$ ]	4.55 [m]

### 2. Numerical Validation

It has been increasingly acknowledged that the numerical modeling of PEM fuel cells performed by FLUENT is extremely precise. An essential performance indicator in the fuel cell flow channel will be the pressure drop that occurs. Validation of the models in this inquiry will be accomplished through a comparison of numerical and analytical pressure drop data.

Flow channel topologies with different geometric characteristics were investigated in this section for two different fuel cell designs. The first geometric arrangement was offered by Atul and Ramana (2002), and the second was provided by Nattawut and Yottana (2011). The numerical simulation results obtained through the use of CFD software will be displayed. Following that, the results of these observations will be compared to previously calculated analytical values.

#### 2.1. Serpentine Channel with Active Area of 4x4 cm<sup>2</sup>

Initially, it is necessary to experiment with a simple structure in order to gain a better understanding of the concept underlying the flow channels in the fuel cell. Using a simple structure allows for easier experimentation. Preliminary verification of the selected simple structure should be done using theory, and then subsequent adjustments can be made to this structure because we will have a solid foundation from which to build on top of it.

##### 2.1.1. Single Serpentine Channel

While conducting a literature review, it became clear that the single serpentine channel was the most frequently experimented with and simulated as a fuel cell flow channel type. It is even considered an industry standard by many scholars and

## RESULTS AND DISCUSSION

companies today. Also known as a yardstick, it is widely used to measure the success of brand-new designs and ideas.

Due to the extensive amount of information available on geometry features, the case study of Atul and Ramana (2002), was chosen. After being meticulously designed on SolidWorks CAD software, the structure was transferred to a computational fluid dynamics (CFD) tool called "ANSYS FLUENT." Then, in order to prepare the model for simulation, the model's fundamental assumptions were established and boundary conditions were imposed. Using the simulation, it was possible to determine the pressure drop values that occurred throughout the channel. To determine whether the findings of the simulation were correct or not, it was necessary to compute the pressure drop using analytical calculations and compare the results with those obtained by the simulations as a last step. All of these stages were repeated for each and every numerical model that will be addressed throughout this study.

In order to begin, let us examine the pressure drop findings of a single serpentine channel obtained using numerical simulation and analytical analysis. With respect to Figure 13, it is pretty evident that, with increasing flow rate, the difference in error between the two techniques of calculating pressure drop increases slightly. Although this inaccuracy is quite small, it is reasonable to conclude that the pressure drop predicted by numerical simulation is in accordance with analytical analysis. Now that it has been properly validated, it is time to make some adjustments in order to see whether it is possible to reduce the pressure drop in this particular "4x4" model.

## RESULTS AND DISCUSSION

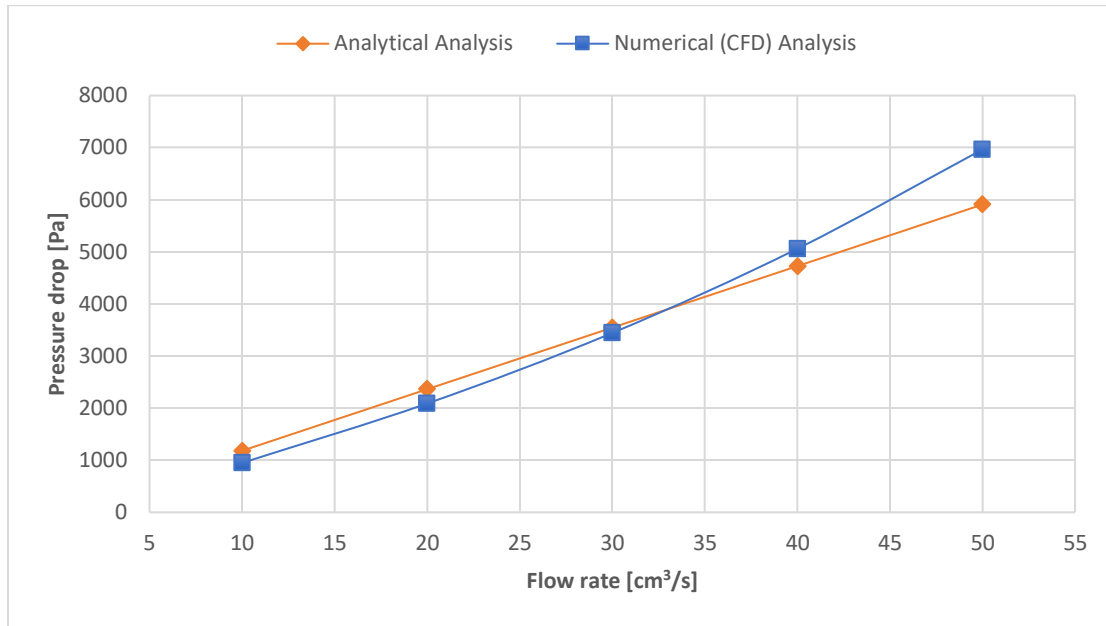
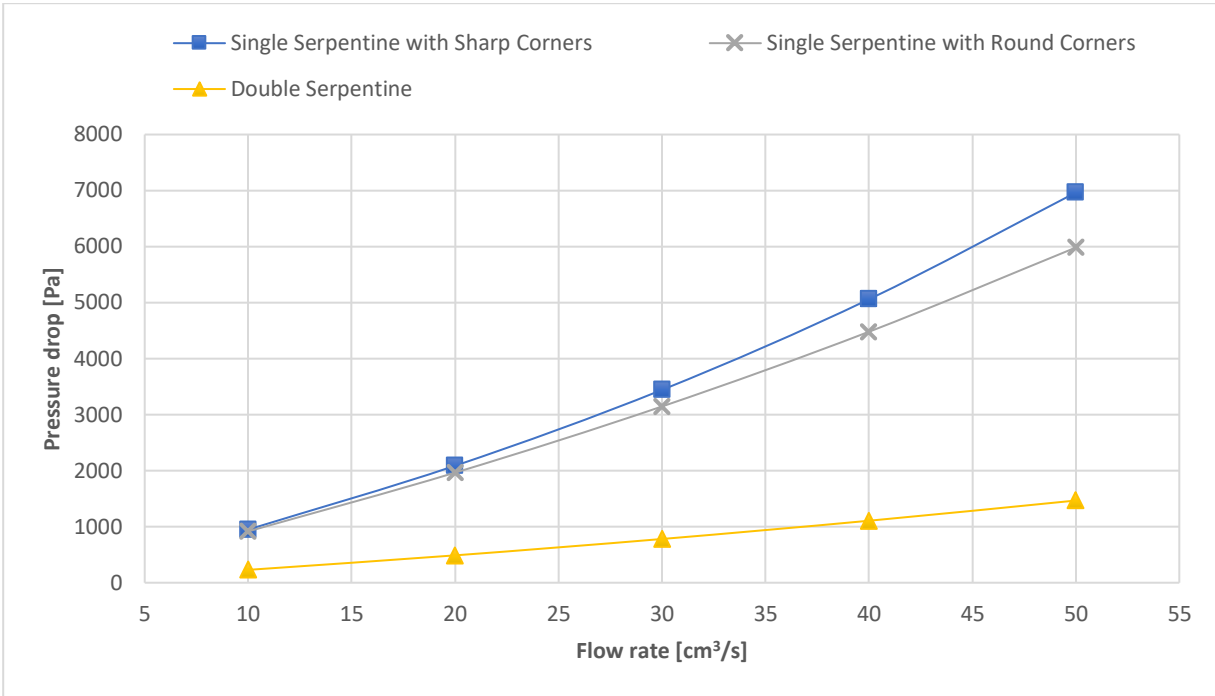


Figure 13. Numerical validation of a single serpentine channel of the "4x4" model with sharp corners.

### 2.1.2. Single Serpentine Channel Modifications

When it comes to the "4x4" model, two major modifications have been performed. As soon as the validity of a single serpentine channel was established, the next logical step was to change the existing sharp corners into round corners. The second adjustment, which was influenced by Nattawut and Yottana (2011)'s case study, was then implemented. They developed flow field channels with double serpentine and triple serpentine configurations. Consequently, it is intended to add an extra inlet and observe how the pressure drop reacts to this change. Furthermore, analytical calculations will be presented too, in order to compare the numerical results provided in Figure 14 with one another.

## RESULTS AND DISCUSSION



*Figure 14. Numerical (CFD) analysis results of pressure drop in different configurations of the "4x4" model.*

On the whole, it is feasible to see from the figure that, while raising flow rate in a systematic way, a gradual increase in pressure drop can be observed in every component of the graph. The presence of a tiny variation between a single serpentine channel and its initial modification, which has rounded corners, is immediately obvious at greater flow rates. That is to say, a single serpentine channel with rounded corners outperforms a single serpentine channel with sharp corners in terms of performance. Compared to the analytical analysis, the outcomes of a single serpentine channel with curvature are nearly identical to the predictions of the theory.

While the noteworthiness is taking place on the double serpentine flow field channel, it is abundantly visible that every pressure drop figure has been reduced by nearly 80% when compared to the analytical calculation of the same flow rate values. Eventually, it is clearly noticeable that the pressure drop values in the selected "4x4"

## RESULTS AND DISCUSSION

model are dropping when modifications are implemented in a controlled CFD simulation environment.

### 2.2. Serpentine Channel with Active Area of 10x10 cm<sup>2</sup>

Until now, only a serpentine channel with a relatively small active area has been investigated. In order to better understand the behavior of the fuel cell flow channel, numerous modifications have been made to the original design. It was immediately apparent that the performance of a single serpentine channel had been improved as a result of the alterations made. It is now time to experiment with the larger active area of a single serpentine fuel cell flow channel. The geometry specifications for the bigger active area of a single serpentine channel were obtained from Nattawut and Yottana (2011) and used for this case.

The case study that was chosen should have all of the relevant input variables and boundary conditions, thus it is critical to double-check this before beginning any numerical simulations. As has been mentioned in the section on model development, the first step consisted of determining which fluid had been implemented, and the second step consisted of computing the pressure drop using analytical calculations and comparing the results with those acquired through simulations.

According to general consensus, three fundamental working fluids, namely hydrogen, oxygen, and water vapor, are capable of being used in PEM fuel cells. Every one of these fluids was carefully modeled in a computational fluid dynamics software, and the pressure drop findings are depicted in Figure 15.

## RESULTS AND DISCUSSION

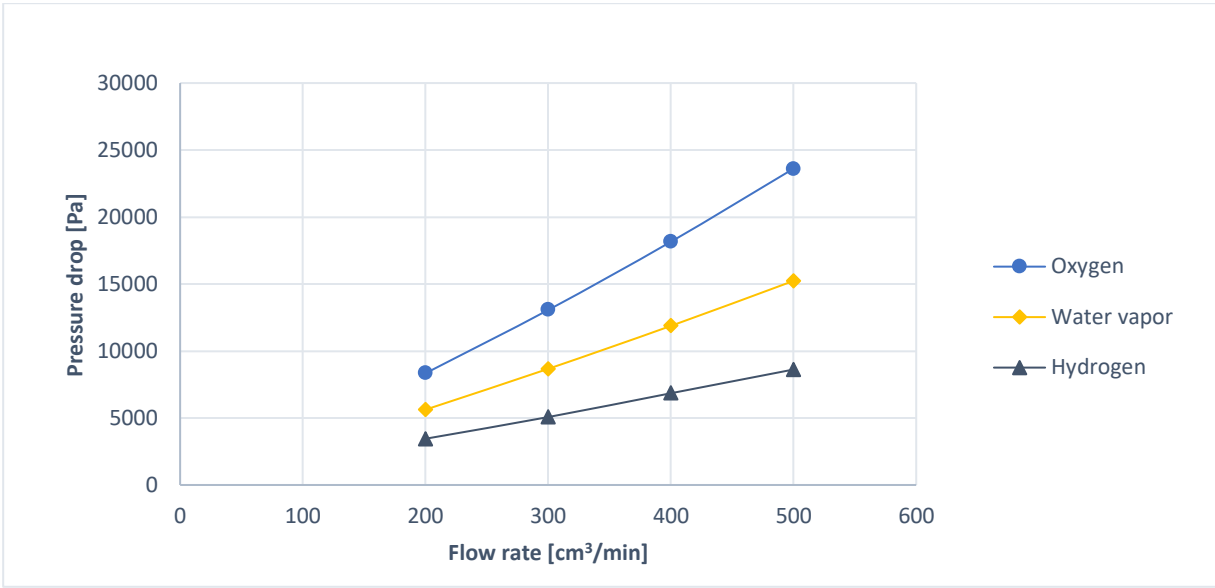


*Figure 15. Numerical (CFD) analysis of "10x10" model pressure drop results for different working fluid.*

As soon as we obtain all of the pressure drop results for each working fluid, it is time to compare them to the results from Nattawut and Yottana (2011)'s study case, especially the data for the sharp curve, in order to determine which fluid was implemented. The pressure drop data from the reference case study is depicted in Figure 16, which makes it clear that the working fluid in this case is oxygen.

## RESULTS AND DISCUSSION

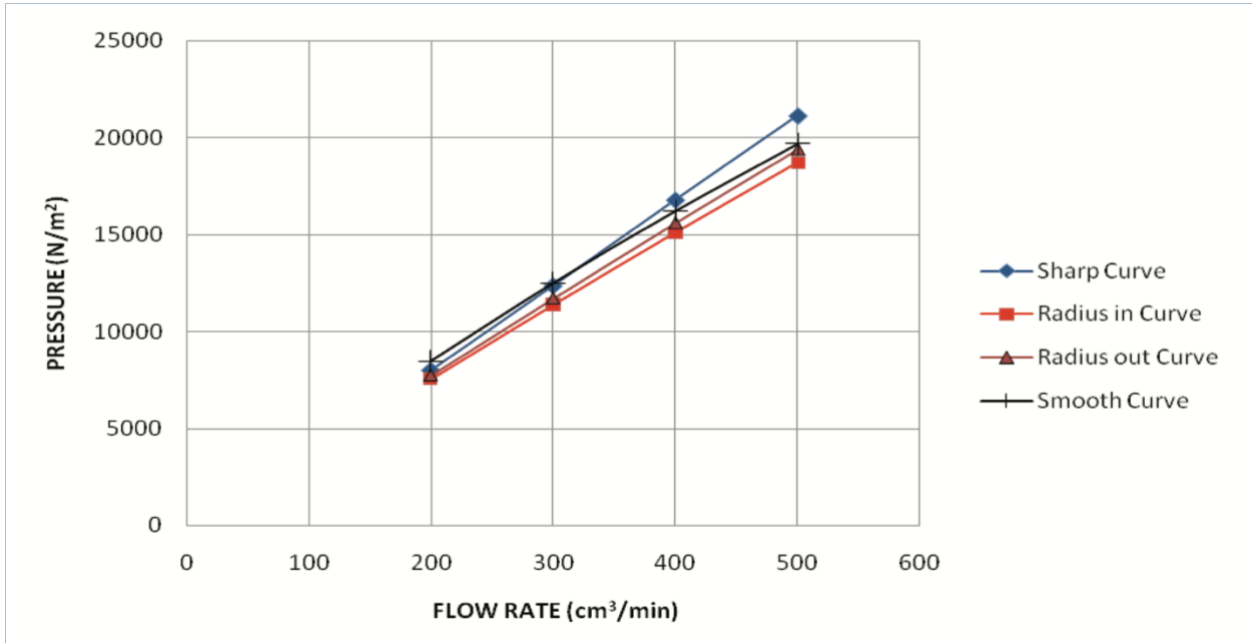
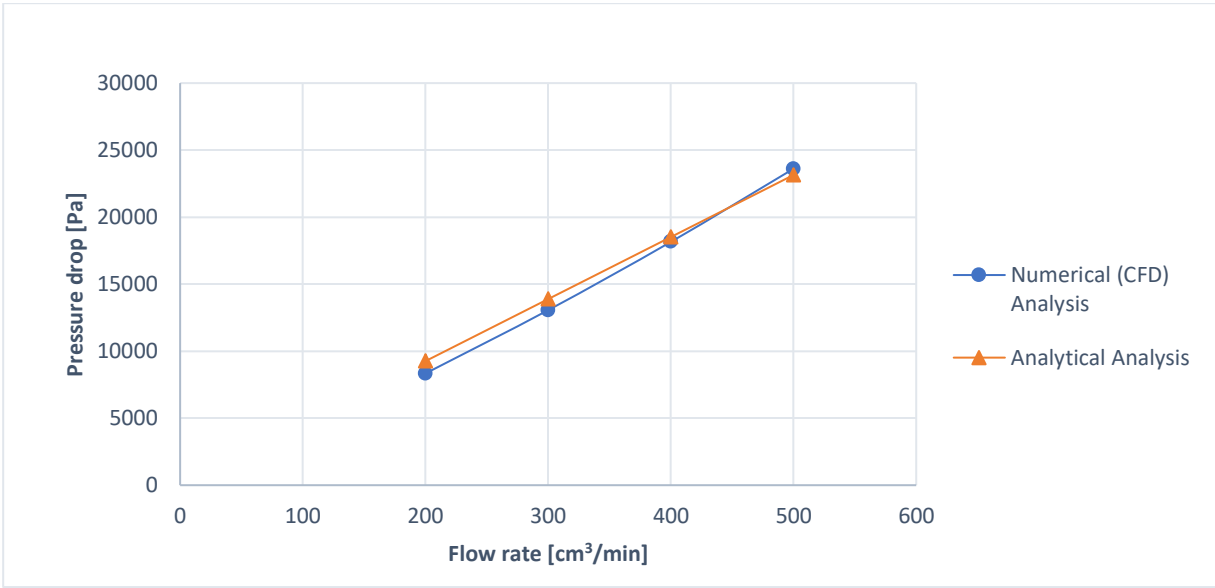


Figure 16. Numerical (CFD) analysis of pressure drop results in different curves [14].

Following the identification of the working fluid that will be employed within the flow channel, the second objective is to confirm that the numerical simulations performed in "FLUENT" are promising. For this particular model, it is necessary to do analytical calculations of pressure drop values in order to proceed with the numerical validation process. Figure 17 depicts these analytical values in conjunction with the results of the CFD investigation. It is readily apparent that the pressure drop values obtained from analytical analysis and simulations are really close. To put it another way, the difference in pressure drop numbers at 500 cm<sup>3</sup>/min is about 8% off, whereas the difference at 200 cm<sup>3</sup>/min is about 4% off. A "10x10" single serpentine channel model with sharp corners has been satisfactorily validated at this point because the provided defects are so tiny.

## RESULTS AND DISCUSSION



*Figure 17. Numerical validation of a single serpentine channel of the "10x10" model with sharp corners and working fluid being oxygen.*

# CONCLUSION

As part of a comprehensive literature review, the benefits and drawbacks of the most widely utilized fuel cell flow channels were examined. In accordance with the literature, a fundamental flow channel design with two different active areas was selected to begin the study: a single serpentine channel with an active area of 4 cm x 4 cm with a rectangular cross section and a single serpentine channel with an active area of 10 cm x 10 cm with a square cross section. The numerical simulation of the PEM fuel cell flow channels and the computation of the resulting pressure drops in the channels were carried out using the commercial ANSYS FLUENT CFD software tool.

The conventional flow channel designs were modified and optimized using ANSYS FLUENT to analyze the impact of the modifications on the channel pressure drops, and new flow channel designs were created. This was taken a step further by examining the pressure drop profiles at various inlet velocities (flow rates). There was a reduction in pressure drop for the majority of the improved designs, which has a positive influence on the fuel cell's overall performance. Studies of mesh independence were performed from the beginning to guarantee that the results were independent of the mesh used for simulation. In addition to peer-reviewed literature, analytical calculations were performed to ensure the accuracy of the data.

Firstly, let's look at the "4x4" model," which has an active area of just four centimeters by four centimeters. In order to improve performance, two adjustments were made to the current "4x4" model after it was validated through an analytical study. According to the simulation results, the redesigned serpentine channel with double inlets had a pressure drop that was five times smaller than the existing single serpentine design. In contrast, the second modified serpentine design with rounded corners only achieved a pressure drop at 50 cm<sup>3</sup>/s with a reduction of only 14% when compared to the existing single serpentine design. To cut a long story short, the modified serpentine

## CONCLUSION

flow channel with a double inlet has the lowest pressure drop of all the modified configurations.

When it comes to the 10 cm x 10 cm active area of the serpentine design, three different working fluids have been simulated: oxygen, hydrogen, and water vapor. Based on the obtained data, it was determined that the working fluid was oxygen, which was confirmed by a comparison with the results of the literature. This was further supported by the results of the analytical analysis.

In terms of the flow uniformity, it is automatically satisfied because, in this study, all the investigated cases have a continuous channel. In the case of the double serpentine channel, there are two continuous channels for each of the two inlets.

This study focused on pressure drop in fuel cell flow channel design, which is a topic that has been discussed extensively in the literature, and how it could be reduced. Additionally, there are numerous other factors that influence the overall performance of any specific fuel cell, including the pressure drop, and more research is required to fully understand the interplay between these numerous parameters and their combined impact on fuel cell efficiency.

## REFERENCES

- [1] M. Muthukumar, P. Karthikeyan, V. Thiagarajan, C. Kim Byung, V. Rajavel, S. Praveenkumar and S. Senthilarasu , Performance Studies of Proton Exchange Membrane Fuel Cells with Different Flow Field Designs – Review, 2021.
- [2] A. Akroot, "Modelling of thermal and water management in automotive polymer electrolyte membrane fuel cell systems," Ankara, 2014.
- [3] J. Ahn, "Control and Analysis of Air, Water, and Thermal Systems for a Polymer Electrolyte Membrane Fuel Cell," 2011.
- [4] F. Barbir, PEM Fuel Cell Theory and Practice, Elsevier, 2005.
- [5] N. Djilali, "Computational modelling of polymer electrolyte membrane (PEM) fuel cells: Challenges and opportunities," *Energy*, 2005.
- [6] J. Zhang, PEM Fuel Cell Electro catalysts and Catalyst Layers Fundamentals and Applications, Springer, 2008.
- [7] A. Hermann, T. Chaudhuri and P. Spagnol, "Bipolar plates for PEM fuel cells: A review," *International Journal of Hydrogen Energy*, 2005.
- [8] A. Arvay, J. French, J.-C. Wang, X.-H. Peng and A. Kannan, "Nature inspired flow field designs for proton exchange membrane fuel cell," *International journal of hydrogen energy*, 2012.
- [9] B. R. Friess and M. Hoorfar, "Development of a novel radial cathode flow field for PEMFC," *International Journal of Hydrogen Energy*, 2012.

## REFERENCES

- [10] K. Atul and R. Ramana G., "Effect of channel dimensions and shape in the flow-field distributor on the performance of polymer electrolyte membrane fuel cells," *Journal of Power Sources*, pp. 11-18, 2002.
- [11] D. Spornjak, A. K. Prasad and S. G. Advani, "In situ comparison of water content and dynamics in parallel, single-serpentine, and interdigitated flow fields of polymer electrolyte membrane fuel cells," *Journal of Power Sources*, vol. 195, no. 11, 2010.
- [12] T. Sherman, "On connecting large vessels to small," *Journal of General Physiology*, vol. 78, no. 4, pp. 431-453, 1981.
- [13] E. Celik and I. Karagoz, "Polymer electrolyte membrane fuel cell flow field designs and approaches for performance enhancement," *Journal of Power and Energy*, vol. 234, no. 8, 2020.
- [14] J. Nattawut and K. Yottana, "Effects of difference flow channel designs on Proton Exchange Membrane Fuel Cell using 3-D Model," 2011.
- [15] J. F. Wendt, *Computational Fluid Dynamics: An Introduction*, Springer, 2008.
- [16] B. R. Munson, T. H. Okiishi and D. F. Young, *Fundamentals of Fluid Mechanics*, 7th ed., 2013.
- [17] Andreas Lintermann, "Computational Meshing for CFD Simulations," 2020.
- [18] L. Xianguo and S. Imran, "Review of bipolar plates in PEM fuel cells: Flow-field designs," *International Journal of Hydrogen Energy*, 2005.

## REFERENCES

- [19] S. A. Ferng Yuh Ming, "A three-dimensional full-cell CFD model used to investigate the effects of different flow channel designs on PEMFC performance," *International Journal of Hydrogen Energy*, 2007.
- [20] E. A. Seyed Ali Atyabi, "Three-dimensional multiphase model of proton exchange membrane fuel cell with honeycomb flow field at the cathode side," *Journal of Cleaner Production*, 2019.
- [21] D. S. Watkins, K. W. Dircks and D. G. Epp, "Novel fuel cell fluid flow field plate". USA Patent 4,988,583, 1991.
- [22] A. Su, F.-B. Weng, C.-Y. Hsu and Y.-M. Chen, "Studies on flooding in PEM fuel cell cathode channels," *International Journal of Hydrogen Energy*, 2006.
- [23] M. S. Hossain, B. Shabani and S. C.P. Cheung, "Enhanced gas flow uniformity across parallel channel cathode flow field of Proton Exchange Membrane fuel cells," *International Journal of Hydrogen Energy*, 2017.
- [24] N. Guo, M. C. Leu and U. O. Koylu, "Bio-inspired flow field designs for polymer electrolyte membrane fuel cells," *International Journal of Hydrogen Energy*, 2014.
- [25] N. Guo, M. C. Leu and U. O. Koylu, "Network based optimization model for pin-type flow field of polymer electrolyte membrane fuel cell," *International Journal of Hydrogen Energy*, 2013.
- [26] N. Cooper, T. Smith, A. D. Santamaria and J. Wan Park, "Experimental optimization of parallel and interdigitated PEMFC flow-field channel geometry," *International Journal of Hydrogen Energy*, 2016.

## REFERENCES

- [27] K. Tüber, A. Oedegaard, C. M. Hebling and M. Hermann, "Investigation of fractal flow-fields in portable proton exchange membrane and direct methanol fuel cells," *Journal of Power Sources*, 2004.
- [28] R. Roshandel, F. Arbabi and G. Karimi, "Simulation of an innovative flow-field design based on a bio inspired pattern for PEM fuel cells," *Renewable Energy*, 2012.
- [29] D. Sandip , S. Sirivatch , Z. JW Van and L. WK, "Effect of humidity on PEM fuel cell performance part II-numerical simulation," 1999.
- [30] J. Scholta, G. Escher, W. Zhang, L. Küppers, L. Jörissen and W. Lehnert, "Investigation on the influence of channel geometries on PEMFC performance," *Journal of Power Sources*, 2004.
- [31] Z. Jianlu, Z. Huamin, W. Jinfeng and Z. Jiujun, *PEM Fuel Cell Testing and Diagnosis*, Elsevier, 2013.
- [32] F. M. White, *Viscous Fluid Flow*, McGraw-Hill, 1974.
- [33] R. K. Shah and A. L. London, *Laminar Flow Forced convection in ducts: A Source Book for Compact Heat Exchanger Analytical Data*, Academic Press, 1978.
- [34] F. Barbir, H. Gorgun and X. Wang, "Relationship between pressure drop and cell resistance as a diagnostic tool for PEM fuel cells," *Journal of Power Sources*, 2004.
- [35] M. Sauer Moser, N. Kizilova, B. G. Pollet and S. Kjelstrup, "Flow Field Patterns for Proton Exchange Membrane Fuel Cells," *Frontiers in Energy Research*, 2020.
- [36] B. R. Alvarado , A. H. Guerrero, D. J. Robles and P. Li, "Numerical investigation of the performance of symmetric flow distributors as flow channels for PEM fuel cells," *International Journal of Hydrogen Energy*, 2011.

## REFERENCES

- [37] J. Dong, S. Liu and S. Liu, "Numerical investigation of novel bio-inspired flow field design scheme for PEM fuel cell," *Journal of Renewable and Sustainable Energy*, 2020.
- [38] D. Jeon, S. Greenway, S. Shimpalee and J. V. Zee, " The effect of serpentine flow-field designs on PEM fuel cell performance," *International Journal of Hydrogen Energy*, 2007.
- [39] D. Ouellette, A. Ozden, M. Ercelik, C. O. Colpan, H. Ganjehsarabi, X. Li and F. Hamdullahpur, "Assessment of different bio-inspired flow fields for direct methanol fuel cells through 3D modeling and experimental studies," *International Journal of Hydrogen Energy*, 2017.
- [40] L. Yuan, Z. Jin, P. Yang, Y. Yang, D. Wang and X. Chen, "Numerical Analysis of the Influence of Different Flow Patterns on Power and Reactant Transmission in Tubular-Shaped PEMFC," *Energies*, 2021.
- [41] M. Marappan, R. Narayanan, K. Manoharan, M. K. Vijayakrishnan, K. Palaniswamy, S. Karazhanov and S. Sundaram, "Scaling up Studies on PEMFC Using a Modified Serpentine Flow Field Incorporating Porous Sponge Inserts to Observe Water Molecules," *Molecules*, 2021.
- [42] A. A. Hmad and N. Dukhan, "Cooling Design for PEM Fuel-Cell Stacks Employing Air and Metal Foam: Simulation and Experiment," *Energies*, 2021.
- [43] A. Arvay, "Proton Exchange Membrane Fuel Cell Modeling and Simulation using Ansys Fluent," 2011.
- [44] V. Velisala and G. N. Srinivasulu, "Numerical Simulation and Experimental Comparison of Single, Double and Triple Serpentine Flow Channel Configuration on Performance of a PEM Fuel Cell," 2017.

## REFERENCES

- [45] P. M. G. Nejad, A. R. S. Nazar, Z. R. Ahar and Z. Karami, "Numerical study on the performance prediction of a proton exchange membrane (PEM) fuel cell," *Iranian Journal of Hydrogen & Fuel Cell*, 2017.
- [46] E. Alizadeh, M. R. Esbo, S. M. Rahgoshay, S. H. Saadat and M. Khorshidian, "Numerical and experimental investigation of cascade type serpentine flow field of reactant gases for improving performance of PEM fuel cell," *International Journal of Hydrogen Energy*, 2017.
- [47] T. Wilberforce, F. N. Khatib, O. Ijaodola , E. Ogungbemi , Z. El-Hassan, A. Durrant , J. Thompson and A. Olabi, "Numerical modelling and CFD simulation of a polymer electrolyte membrane (PEM) fuel cell flow channel using an open pore cellular foam material," *Science of the Total Environment*, 2019.